Journal of Electron Spectroscopy and Related Phenomena 235 (2019) 60–67

Contents lists available at ScienceDirect

Journal of Electron Spectroscopy and Related Phenomena

journal homepage: www.elsevier.com/locate/elspec

Influence of multipole effects on the cross section and alignment following inner-shell ionization of atoms by a linearly polarized photon

Zhan-Bin Chen[a,1], Kun Ma[b,1,*], Cui-Cui Sang[c], Xiang-Li Wang[d], Kai Wang[e]

[a] Department of Applied Physics, School of Science, Hunan University of Technology, Zhuzhou 412007, China
[b] School of Information Engineering, Huangshan University, Huangshan 245041, China
[c] College of Science, Lanzhou University of Technology, Lanzhou 730050, China
[d] Key Laboratory for Electronic Materials of the State Ethnic Affairs Commission, College of Electrical Engineering, Northwest Minzu University, Lanzhou 730030, China
[e] Hebei Key Lab of Optic-electronic Information and Materials, The College of Physics Science and Technology, Hebei University, Baoding 071002, China

ARTICLE INFO

Keywords:
Alignment
Multipole effects
Linearly polarized light

ABSTRACT

On the basis of the fully relativistic Dirac-Fock treatment of single ionization by a linearly polarized photon with regard to the $E1$, $M1$, $E2$, $M2$, and $E3$ multipoles of the radiative field as well as their interference, we have assessed the influence of multipole effects on the cross sections and alignment parameters A_{20} and A_{22} of the residual ions, taking the $3p_{3/2}$ and $3d_{3/2}$ vacancies of selected Zn and Zn-like Kr^{6+}, Cd^{18+}, and Xe^{24+} ions as examples. Starting from the most general method of density matrix theory, we carried out specific analytic expressions in terms of the reduced matrix elements of multipole fields, corresponding to different ion-core states. It is shown that the multipole contributions to the photoionization cross sections can be considerable, the character of which becomes more evident as the incident energy and/or atomic number increases. These dramatic influences also lead to a remarkable increase in the alignment parameter A_{20} of the residual ions, yet virtually independent of the nuclear charge for A_{22}. The present results in Coulomb gauge and Babushkin gauge excellently agreed with each other, suggesting that there is a high degree of convergence achieved in this study. Comparison of our results with experimental data and other theoretical predictions, when available, is made.

1. Introduction

Photoionization (PI) is a basic atomic process and widely exists in laboratory and astronomical plasmas [1–6], such as fusion device [7], solar corona [8] and so on. Studies regarding PI of atomic ions led to a fundamental understanding of atomic interactions. With the rapid development of the high photon flux of third-generation synchrotron radiation sources and the photon-ionmerged-beams technique, facilitating measurements at an unprecedented level of refinement and precision, experiments on inner-shell PI of atomic ions have become possible. For the inner-shell PI, it produced a vacancy state in the residual ion. Flügge et al. [9] pointed out that if the residual ion is with total angular momentum $J > 1/2$, the ion will be aligned with respect to the direction of incident photon. Since alignment is a measurable quantity, it provides information on the process of ionization and the wave function of electron, and results in a more sensitive testing for the validity of the approximate methods.

On the experimental side, first evidence for an alignment resulting from inner-shell PI in Cd 4d was discovered by Caldwell and Zare using He I resonance radiation [10]. Later, more accurate experiments were carried out by using X-ray lasers [11] or synchrotron radiation and coincidence techniques for the inner-shell vacancies of atoms. Kahlon et al. [12] observed alignment of the L_3 subshell vacancy state produced after PI in lead by photons. Küst et al. [13] measured alignment of Xe^+ ion after L_3 PI via the anisotropy of L*l* X-radiation using linearly polarized synchrotron radiation. Their results were smaller in magnitude by roughly a factor of 2-3 than the theoretical ones within the Hartree-Fock (HF) approximation. Kronast et al. [14] measured alignment parameters of the residual ions Cd^+ ($4d^{-1}_{5/2,3/2}$) and Zn^+ ($3d^{-1}_{3/2}$) using synchrotron radiation, and their data were in good agreement with theoretical results. Özdemir et al. [15] determined the alignment parameters of some heavy elements induced by photons. The others reported alignment measurements include alkaline earth metals [16,17], the transition metals [18,19] as well as the rare gases [20,21].

On the theoretical side a fair number of studies have been done using different approaches. Kleiman and Lohmann [22] provided a

* Corresponding author.
E-mail address: makun0602@163.com (K. Ma).
[1] These authors contributed equally to this work.

https://doi.org/10.1016/j.elspec.2019.07.003
Received 10 October 2018; Received in revised form 7 May 2019; Accepted 9 July 2019
Available online 31 July 2019
0368-2048/

theoretical study on the orientation and alignment parameter for the PI of atoms by applying a relaxed orbital method within a single-configurational HF approach. Later, they proposed a method for calculating alignment for open shell atoms after PI [23]. Berezhko et al. [24] calculated alignment of the $3p_{3/2}$ shell of Ge. Based on the first order perturbation theory, Vorobyev et al. [25] proposed a quantum mechanical treatment for calculating the production cross section and alignment of inner-atomic-shell vacancies induced by photon or ion impact. Theoretical values of the alignment parameters for different states of various atoms calculated using the Herman-Skillman wave functions have been reported by Berezhko and Kabachnik [26]. Recently, Sharma et al. [27] calculated alignments of some high Z elements by using the non-relativistic electric dipole ($E1$) approximation in a point Coulomb potential and analytical perturbation theory in a screened Coulomb potential. Their results were compared with available theoretical and experimental values. There were also many other studies regrading the alignment of the residual ion [28–31].

For a long time, the $E1$ approximation is satisfied in PI due to the photon at low energy. The $E1$ approximation assumes that the radiation field, i.e., the plane wave expanded in a Taylor series as $\exp(\mathbf{i}\mathbf{k}\cdot\mathbf{r}) \approx 1 + \mathbf{i}\mathbf{k}\cdot\mathbf{r} - \frac{1}{2}(\mathbf{k}\cdot\mathbf{r})^2 + \cdots$, can be truncated to unity. In this situation, all higher order multipole interactions, like electric quadrupole, magnetic quadrupole, etc., are neglected. Some recent studies convincingly demonstrate the breakdown of the $E1$ approximation and provide sufficient quantitative data to initiate detailed new theoretical investigations of PI process at higher energies, where the $E1$ approximation is no longer valid. Inal et al. [32] calculated higher-order effects on the linear polarization of the characteristic X-ray radiation following the inner-shell PI of highly charged ions. Bechler and Pratt [33] investigated higher multipole and retardation corrections to the dipole angular distributions of L-shell photoelectrons ejected by polarized photons. Cooper [34] evaluated multipole corrections to the angular distribution of photoelectrons at low energies. Other reports can be found in Refs. [30,35–40]. These authors discussed the influence of nondipole effects on the different PI parameters.

In the present work, we turn our attention to filling in aspects of the problem which so far have been unexplored, that is, multipole effects on the alignment parameters of the residual ions after inner-shell ionization by a linearly polarized light, taking the $3p_{3/2}$ and $3d_{3/2}$ vacancies of Zn and Zn-like Kr^{6+}, Cd^{18+}, and Xe^{24+} ions as examples. For this purpose, the fully relativistic method for treating the PI process is developed, based on the density matrix theory [41]. In this method, the target state wave functions are generated in the framework of the self-consistent Dirac-Fock method [42–50]. The continuum wave function of the projectile electron is obtained by solving the Dirac equations. To perform the analysis, we computed two sets of alignment parameters, respectively, within the relativistic $E1$ approximation and the relativistic theory which includes significant multipole orders of the radiative field. Results are compared in order to stress the importance of multipole effects as the atomic number and/or incident energy increases. Comparison with available experimental and theoretical results is also made. The layout of this paper is as follows. The theoretical framework of our method is presented briefly in Section 2, where essential formulas are derived and the observables are introduced. Section 3 presents a discussion and a comparison of our results with other available experimental data and theoretical predictions. The conclusion is eventually drawn in Section 4.

2. Theoretical method

The single PI process can be expressed as

$$\hbar\omega + A^{q+}(\alpha_i J_i) \rightarrow A^{q+1}(\alpha_f J_f) + e_{\rm ph}, \tag{1}$$

where the subscript i/f denotes the initial/final ionic states of the PI process [2]. J and α represents, respectively, the corresponding total angular momentum quantum number and additional quantum numbers required for an unique specification of the state. Apart from the conventional observable cross section, the alignment studies are found to be much more effective with regard to the details of the various effects and, in fact, helped provide newinsight into the electron-photon (*e-ph*) interactions in the presence of strong Coulomb fields. Theoretically, the formation and alignment of excited ions are treated separately [32,51–53]. Most conveniently, such a treatment is performed within the framework of the density-matrix theory [41]. A concise description of such theory has been discussed in detail by Inal et al. [32] and Kämpfer et al. [51]. Therefore, only a brief account will be given here. In the density matrix theory, for the PI of atoms or ions by a light beam that propagates along the quantization x axis, if the photoelectron remains unobserved, then the statistical tensor of the photoion is presented by [32,51–53]

$$\begin{aligned}\rho_{\rm kq}(\alpha_f J_f) = \frac{\pi}{2J_i+1}\sum_{\rm LL'pp'}\sum_{\kappa \rm JJ'}\sum_{\lambda\lambda'} i^{L-L'+p-p'}\lambda^p\lambda'^{p'}[\rm LL'JJ']^{1/2}[\delta_{\lambda\lambda'} \\ + (1-\delta_{\lambda\lambda'})P^{\rm in}] \\ \times(-1)^{J+J'+J_f+J_i+j+1} < L\lambda L' - \lambda'|\rm kq > \begin{Bmatrix} J_f & j & J' \\ J & k & J_f \end{Bmatrix}\begin{Bmatrix} J' & J_i & L' \\ L & k & J \end{Bmatrix} \\ \times < (\alpha_f J_f, \varepsilon\ell j)J||H_\gamma(\rm pL)||\alpha_i J_i > < (\alpha_f J_f, \varepsilon\ell j)J'||H_\gamma(p'L')||\alpha_i J_i >^* .\end{aligned} \tag{2}$$

In the expression above, $P^{in} = 0/P^{in} = 1$ represents the unpolarized/polarized incoming light beam. $[ab\ldots] = (2a+1)(2b+1)\ldots$, and the standard notation for the Clebsch-Gordan coefficients and the Wigner 6-j symbols have been utilized. $\vec{\alpha}$ denotes the Dirac matrices, and $\lambda = \pm 1$ is the helicity, which is the projection of the photon spin on its linear momentum. $\kappa = \pm(j+1/2)$ for $\ell = j \pm 1/2$, which is the Dirac angular momentum. The standard notations are the reduced matrix elements of multipole fields, which describe the *e-ph* interaction of an ionic bound state with the (one-electron) continuum of the next higher charge state [32,52,53], given by

$$<(\alpha_f J_f, \varepsilon\ell j)J||H_\gamma(\rm pL)||\alpha_i J_i> = i^{-l}e^{i\Delta\kappa} < (\alpha_f J_f, \varepsilon\ell j)J||\sum_n \vec{\alpha}_n\cdot\vec{A}^{\,p}_{L,n}||\alpha_i J_i> , \tag{3}$$

where $\Delta\kappa$ is phase shift of emitted electron. $\sum_n \vec{\alpha}_n\cdot\vec{A}^{\,p}_{L,n}$ is the transition operator, which describes the relativistic *e-ph* interaction. $\vec{A}^{\,p=0,a}_{L,n}$ is expressed in terms of the electric($p=1$)/magnetic($p=0$) multipolarities components.

The reduced statistical tensors are referred to as the alignment parameters $A_{kq}(\alpha_f J_f)$, which are independent of the particular normalization of the density matrix [32,51,52]

$$A_{\rm kq}(\alpha_f J_f) = \frac{\rho_{\rm kq}(\alpha_f J_f)}{\rho_{00}(\alpha_f J_f)}, \tag{4}$$

where $A_{k0}(\alpha_f J_f)$ are directly related to the partial cross sections σ_{Mf} for the population of the individual ionic substates

$$A_{k0}(\alpha_f J_f) = \frac{\sqrt{2J_f+1}}{\sigma(\alpha_f J_f)}\sum_{M_f}(-1)^{J_f-M_f} < J_f M_f J_f - M_f|k0 > \sigma(M_f), \tag{5}$$

in which

$$\sigma(\alpha_f J_f) = \sum_{M_f}\sigma(M_f) = \frac{8\pi^3\alpha}{\omega(2J_i+1)}\sum_{\kappa \rm J\,Lp} |< (\alpha_f J_f, \varepsilon\ell j)J||H_\gamma(\rm pL)||\alpha_i J_i > |^2. \tag{6}$$

Here, if the rank k is even and $k \le 2J_f$, the alignment parameters $A_{kq}(\alpha_f J_f)$ are nonvanishing. Moreover, for each $k \ge 2$, only the components with $q = 0$ and $q = 2$ may appear to be nonzero. The two components with $q = \pm 2$ are proportional to P^{in} and, hence, vanish/nonzero for ionization by an unpolarized/polarized photon beam.

3. Calculations and discussions

From Eqs. (2) to (5), it is clearly that all the alignment parameters can be traced back to the computations of the (multipole) many-electron amplitudes $<(\alpha_f J_f, \varepsilon\ell j)J||\sum_n \vec{\alpha}_n \cdot \vec{A}^p_{L,n}||\alpha_i J_i>$, or rather, the matrix element $<(\alpha_f J_f, \varepsilon\ell j)J||H_\gamma(pL)||\alpha_i J_i>$. In the present work, calculations of the initial- and final-state wave functions for target atoms/ions considered require the simultaneous consideration of electronic correlations and relativistic effects. The multiconfiguration Dirac-Fock (MCDF) method implemented in the GRASP2K code is ideal for this purpose [54–62]. In most standard computations, the configuration state functions are built from products of one-electron Dirac orbitals. Then, the angular data for the optimization of radial orbitals for the energy expression of multi-configuration wave function in the Dirac-Coulomb approximation are generated. After that, both the radial parts of the Dirac orbitals and the expansion coefficients of states are optimized to self-consistency by solving the MCDF equations in the relativistic self-consistent field procedure. Finally, the relativistic configuration interaction approach is using a fixed pre-optimized set of orbitals and allowing only the mixing coefficients to be varied. During the computation, the Breit interaction and leading quantum electrodynamical effects can be taken into account perturbatively as well [54].

To calculate the PI amplitudes, the continuum wave functions are generated by the component COWF of RATIP package [63] by solving the coupled Dirac equation in which the exchange effect between the bound and free electron are considered. For the continuum functions, orthogonality is enforced with respect to the bound-state orbitals of the same symmetry. However, for different symmetries of the continuum orbitals and different J, orthogonality is obtained automatically. The normalization is determined by a WKB method [63]. The corresponding matrix element/cross section is calculated using a newly fully relativistic program, recently developed by us, based on the PHOTO component of the development version of the RATIP package [63].

In order to verify the modification of the computer packages and check our numerical method, our calculated alignment A_{20} for the $4d^{-1}_{5/2}$ state following PI of Xe atom by a linearly polarized photon is listed, along with available results from other theoretical calculations [24] and experimental values [64–69] in the literature. In our calculation, the $E1$, $M1$, $E2$, $M2$, and $E3$ multipoles of the radiative field and their interference are included. On inspection, the overall agreement is good. Our results are slightly bigger than the experimental data [64–69], and agree with the calculation involving the Herman-Skillman wavefunctions and the calculation involving the HF wavefunctions reported by Berezhko et al. [24] quite well. Especially at the intermediate energy range, the present results lie between these previous calculations. Moreover, the present results in Coulomb gauge and Babushkin gauge agree well with each other, suggesting that there is a high degree of convergence achieved in the present study (Fig. 1).

The main concern of most PI researches is the cross section. For the direct ionization of the $3p_{3/2}/3d_{3/2}$ subshell for Zn and Zn-like Kr^{6+}, Cd^{18+}, and Xe^{24+} ions, our calculated ionization energies IE are, respectively, 99.66/14.93, 219.84/93.48, 630.49/419.41, and 946.46/688.62 eV. Table 1 lists the total cross sections for PI of Zn and Zn-like Kr^{6+}, Cd^{18+}, and Xe^{24+} ions initially in their ground state to the inner-shell $3p_{3/2}$ and $3d_{3/2}$ vacancies for various incoming photon energies in multiples of the IE. Though incoming energies up to 32IE have been considered, only those energy regions in which the cross sections markedly vary are shown. For illustrating the effects which arise from the higher (nondipole) multipoles in the expansion of the *e-ph* interaction, here, calculations have been performed for two kinds of cross sections. The calculations are first made using the relativistic $E1$ approximation (labeled as $E1$). Then, calculations are made using the relativistic treatment with multipoles of the radiation (labeled as MP). In this case, the $E1$, $M1$, $E2$, $M2$, and $E3$ multipoles of the radiative field and their interference were taken into account. Inspection of Table 1 shows that the behavior for increasing energies of cross sections with and with-out multipole effects remains approximately the same. That is to say, the PI cross sections increase sharply with increasing incoming photon energy before starting to decrease, and reach their maximum near the threshold. An interesting feature, exhibited for all ions in the present study, is the shift of peak structure to lower incoming energies as the Z increases. The multipole contributions to the PI cross sections against incoming photon energy are further given in Fig. 2. As expected, for Zn, differences between the MP and $E1$ cross sections are weak. They do not exceed 1% even at 32IE, yet for Xe^{24+} ion, the MP results differ significantly from the $E1$ ones. Taking the inner-shell $3p_{3/2}$ vacancy as an example, at an incoming photon energy of 6IE, the MP result leads to an increase in the cross section by a factor of 0.01 for compared to calculations in the $E1$ case, while At 32IE, the effects of multipole lead to a considerable increase for cross section, which could reach 15% of the $E1$ results. For a given ion, multipole effects in cross section for PI different shells are different. For example, for Xe^{24+} ion, the effect of the multipole on the cross section is about 30% and 14% for $3d_{3/2}$ and $3p_{3/2}$ PI at 32IE, respectively.

Besides the cross section, the alignment of the excited ion states, i.e, A_{20} and A_{22}, are also affected by the multipoles effects (As stated in section 2, the incoming light polarization leads to a nondiagonal density matrix, and, as a result, to a nonvanishing parameter A_{22}). Fig. 3 shows the A_{20} and A_{22} of $3p_{3/2}/3d_{3/2}$ vacancy of Zn and Zn-like Kr^{6+}, Cd^{18+}, and Xe^{24+} ions after PI as a function of incoming photon energy. Inspecting the structure of A_{20} and A_{22}, it becomes evident that the alignments depend on the dynamics of the PI process. The A_{20} reaches large values where the PI cross section is small. For the $3p_{3/2}$ vacancy of Zn, the A_{20} curve has two peaks near-threshold, and at incoming photon energy > 4IE, it remains practically constant. For the $3p_{3/2}$ vacancy of Kr^{6+} ion, the value of A_{20} decreases rapidly from threshold. The value A_{20} of Xe^{24+} ion remains practically constant throughout the energy region covered, yet a rapid change in the A_{20} near threshold is found for Cd^{18+} ion. Comparing the results of the calculations for the $3p^{-1}_{3/2}$ and $3d^{-1}_{3/2}$ states for a given ion, one notices an decrease in the width of the curve dip as one goes to higher subshells. The reason behind this is the fact that with increasing orbital quantum number, the wavefunctions of the electrons in the atom/ion become less compact. The position of the peak and/or dip of the A_{22} curve is the same as A_{20} curve, yet the value is opposite. Furthermore, calculations of the multipole contributions to the alignment parameters of Zn and Zn-like Kr^{6+}, Cd^{18+}, and Xe^{24+} ions are given in Fig. 4, where we can see that in all cases the multipole contributions result in an enhancement of the alignment A_{20}. Strongest multipole effect arises, of course, for the highest photon energy 32IE for which the alignment A_{20} is increased by almost 0.6% (6.1%), 3.6% (15.5%), 14.2% (43.8%), and 22.2% (62.1%), respectively, for the $3p_{3/2}(3d_{3/2})$ vacancy of Zn and Zn-like Kr^{6+}, Cd^{18+}, and Xe^{24+} ions, if the higher multipoles are taken into account. Similarly, for the alignment A_{22}, multipoles effects increase by almost 1.50% (0.054%), 3.46% (0.078%), 8.83% (0.23%), and 12.2% (0.62%) for the $3p^{-1}_{3/2}(3d^{-1}_{3/2})$ state of the above ions at 32IE, respectively.

The Z-dependence of the multipole effect at a given incoming photon energy can more clearly be seen in Fig. 5, which shows the alignment parameters with and without the multipole effects included as functions of the atomic number at 25IE. Obviously, the alignment parameters which rapidly increase as the atomic number increases show a strong dependence on the atomic number. This is particularly true for the A_{20} of the $3d_{3/2}$ vacancy of Xe^{24+} ion, for which inclusion of multipole effects increase the A_{20} deviations by about 55%.

Finally, we would like to say a few words on how the multipole effects significantly alter the PI cross sections and the alignment parameters. To explore the nature of such influences, a set of the module of the reduced matrix element $T = \langle(\alpha_f J_f, \varepsilon\ell j)J||H_\gamma(pL)||\alpha_0 J_0\rangle$, for mainly PI channel against incoming photon energy for the $3d_{3/2}$ vacancy of Xe^{24+} ion are given in Fig. 6. It is clear from the figure that the main contribution to the PI cross section of $3d_{3/2}$ shell comes from the $f_{5/2}$

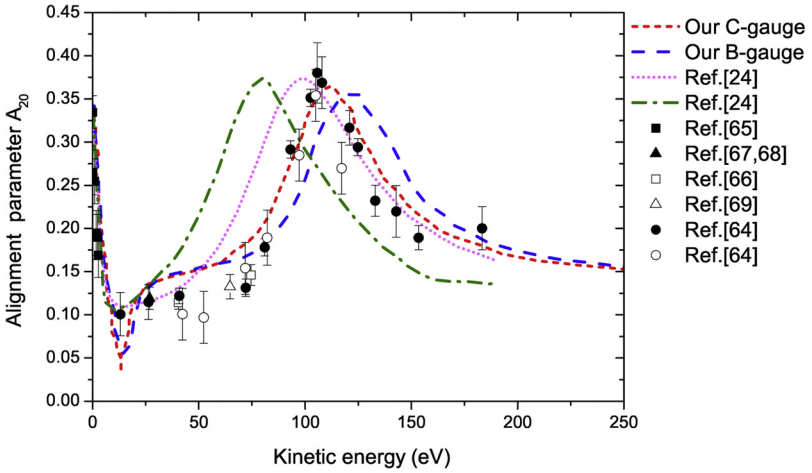

Fig. 1. Comparison of the alignment parameter A_{20} for Xe^+ ion with a vacancy in the $4d_{5/2}$ subshell as a function of the photoelectron energy (in eV). The dot curve is a calculation involving the Herman-Skillman wavefunctions [24], the dash dot curve is a calculation involving the Hartree-Fock wavefunctions [24].

channel. The second largest contribution is the $p_{1/2}$ channel. For each channel, the module of the reduced matrix element rapidly decrease as the incoming photon energies increases. Furthermore, to find which multipole produces the larger effect, our calculated alignment parameters for $3d_{3/2}^{-1}$ state of Xe^{24+} ion using the same method with the $E1$ and magnetic-dipole ($M1$) terms (labeled by $E1+M1$) and with the $E1$, $M1$ and electric-quadrupole ($E2$) terms included in the multipole expansion of the radiation field (labeled by $E1+M1+E2$) are shown in Fig. 7, where we can see that the $E2$ term has a considerable influence on the alignment parameters A_{20} and A_{22}, and that the resulting changes become progressively more significant as the incoming photon energy increases. The performed partial analysis clearly demonstrates that the multipoles corrections provide the dominant contributions beyond the $E1$ approximation in PI.

In the above study, we restricted the investigation to the $E1$, $M1$, $E2$, $M2$, and $E3$ multipoles of the radiative field as well as their interference on the PI process. Note also, that these effects will not only be seen in cross sections and alignment parameters, but in other PI parameters as well, e.g, spin-polarization parameters. Moreover, admittedly, higher-order effects such as the En and Mn ($n > 3$) multipoles may play significant roles in some cases. However, according to our estimates, these corrections to the alignment parameters of the ions of interest are relatively small (less than 0.01%) and thus are neglected in the present calculations, which could be a good approximation for the purposes of discussing the contributions of the multipole to the alignment of residual ions.

4. Conclusion

To summarize, in the present study, a complete set of alignment parameters, namely A_{20} and A_{22}, after PI of Zn and Zn-like Kr^{6+}, Cd^{18+}, and Xe^{24+} ions by a linearly polarized photon have been reported. The calculations have been done by applying a newly developed fully relativistic method, where the target states are determined using fully

Table 1
The $3p_{3/2}$ and $3d_{3/2}$ PI total cross section (in barns) for Zn and Zn-like Kr^{6+}, Cd^{18+} and Xe^{24+} ions. The rows labeled by E1 and MP stand for the values calculated within the relativistic $E1$ approximation and the relativistic theory includes the multipoles in the *e-ph* interaction, respectively. Here IE represents the ionization energy.

State	Incoming energy	Zn (E1)	Zn (MP)	Kr^{6+} (E1)	Kr^{6+} (MP)	Cd^{18+} (E1)	Cd^{18+} (MP)	Xe^{24+} (E1)	Xe^{24+} (MP)
$3p_{3/2}$	1.1IE	3.816E−01	3.817E−01	3.094E−01	3.095E−01	2.694E−01	2.707E−01	2.103E−01	2.117E−01
	1.5IE	2.390E−01	2.394E−01	4.093E−01	4.101E−01	2.344E−01	2.351E−01	1.555E−01	1.559E−01
	1.8IE	3.513E−01	3.519E−01	3.951E−01	3.959E−01	1.836E−01	1.839E−01	1.166E−01	1.168E−01
	2.0IE	3.971E−01	3.977E−01	3.601E−01	3.607E−01	1.434E−01	1.435E−01	9.686E−02	9.695E−02
	2.5IE	4.297E−01	4.303E−01	2.824E−01	2.827E−01	1.011E−01	1.012E−01	6.863E−02	6.866E−02
	3.0IE	4.113E−01	4.117E−01	2.277E−01	2.278E−01	7.346E−02	7.348E−02	4.339E−02	4.342E−02
	3.5IE	3.597E−01	3.600E−01	1.842E−01	1.843E−01	5.502E−02	5.504E−02	3.302E−02	3.307E−02
	4.0IE	3.137E−01	3.138E−01	1.364E−01	1.364E−01	3.873E−02	3.878E−02	2.279E−02	2.285E−02
	5.0IE	2.345E−01	2.345E−01	9.451E−02	9.453E−02	2.444E−02	2.451E−02	1.335E−02	1.343E−02
	10.0IE	6.577E−02	6.580E−02	2.090E−02	2.096E−02	3.970E−03	4.040E−03	2.130E−03	2.200E−03
	15.0IE	2.591E−02	2.597E−02	8.090E−03	8.150E−03	1.390E−03	1.430E−03	6.475E−04	6.832E−04
	25.0IE	6.920E−03	6.960E−03	1.610E−03	1.640E−03	2.609E−04	2.790E−04	2.270E−04	2.467E−04
	32.0IE	3.810E−03	3.840E−03	8.009E−04	8.233E−04	1.286E−04	1.404E−04	6.254E−05	7.156E−05
$3d_{3/2}$	1.1IE	1.140	1.140	2.378E−01	2.379E−01	9.468E−01	9.468E−01	9.965E−01	9.966E−01
	1.5IE	1.718	1.718	1.320	1.320	9.201E−01	9.203E−01	5.154E−01	5.158E−01
	1.8IE	2.094	2.094	1.860	1.860	6.377E−01	6.382E−01	3.422E−01	3.427E−01
	2.0IE	2.402	2.402	1.896	1.897	4.862E−01	4.868E−01	2.552E−01	2.558E−01
	2.5IE	2.728	2.728	1.665	1.665	2.578E−01	2.584E−01	1.493E−01	1.499E−01
	3.0IE	2.963	2.963	1.393	1.393	1.642E−01	1.648E−01	8.037E−02	8.093E−02
	4.0IE	3.050	3.051	7.891E−01	7.895E−01	7.567E−02	7.614E−02	2.949E−02	2.987E−02
	5.0IE	2.926	2.926	4.768E−01	4.773E−01	3.430E−02	3.464E−02	1.326E−02	1.352E−02
	10.0IE	1.868	1.868	6.904E−02	6.931E−02	3.320E−03	3.410E−03	1.640E−03	1.720E−03
	15.0IE	9.842E−01	9.846E−01	2.345E−02	2.361E−02	8.401E−04	8.807E−04	2.788E−04	3.029E−04
	25.0IE	3.411E−01	3.414E−01	4.180E−03	4.240E−03	1.272E−04	1.384E−04	4.685E−05	5.382E−05
	32.0IE	1.785E−01	1.788E−01	1.390E−03	1.430E−03	3.398E−05	3.838E−05	1.898E−05	2.266E−05

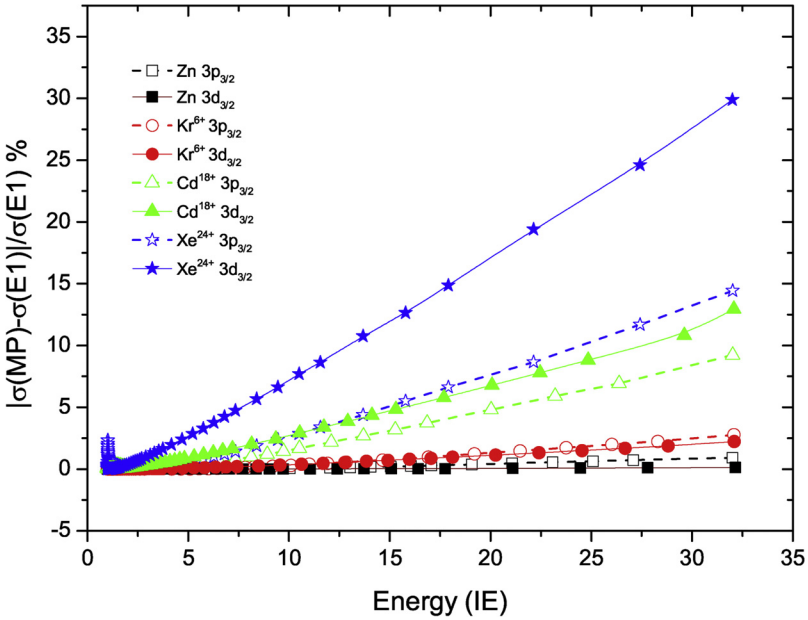

Fig. 2. Plot of the relative multipole contributions to the PI cross sections against incoming photon energy.

relativistic MCDF wave functions with the inclusion of the Breit interaction and the leading quantum electrodynamical effects. The PI amplitudes are calculated based on the PHOTO component of the development version of the RATIP package [63]. Incoming photon energies up to at least 32IE have been considered. The energy dependence of the cross sections/alignment parameters, which basically manifests itself in characteristics of the corresponding curves, has been touched on. From the comparison of our calculations, based on the *E*1 approximation and the MP approximation, we find that the higher multipoles of the radiation field typically lead to an enhancement of both the cross sections and the alignment parameters for all the ions. Also, the computed relative contributions from nondipole interactions to the cross sections/

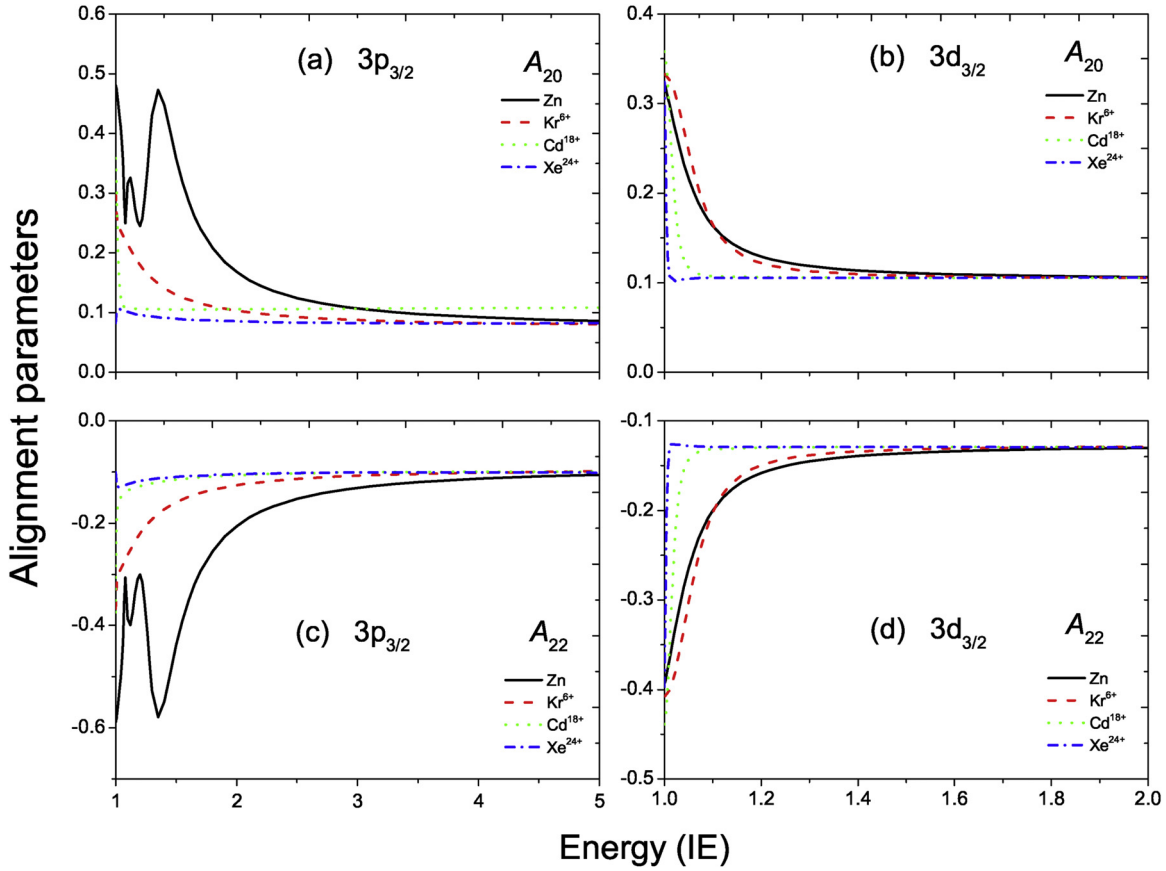

Fig. 3. Plot of the alignment parameters after PI of Zn and Zn-like Kr^{6+}, Cd^{18+} and Xe^{24+} ions by a linearly polarized photon against incoming photon energy. The calculations are made using the relativistic treatment with multipoles of the radiation.

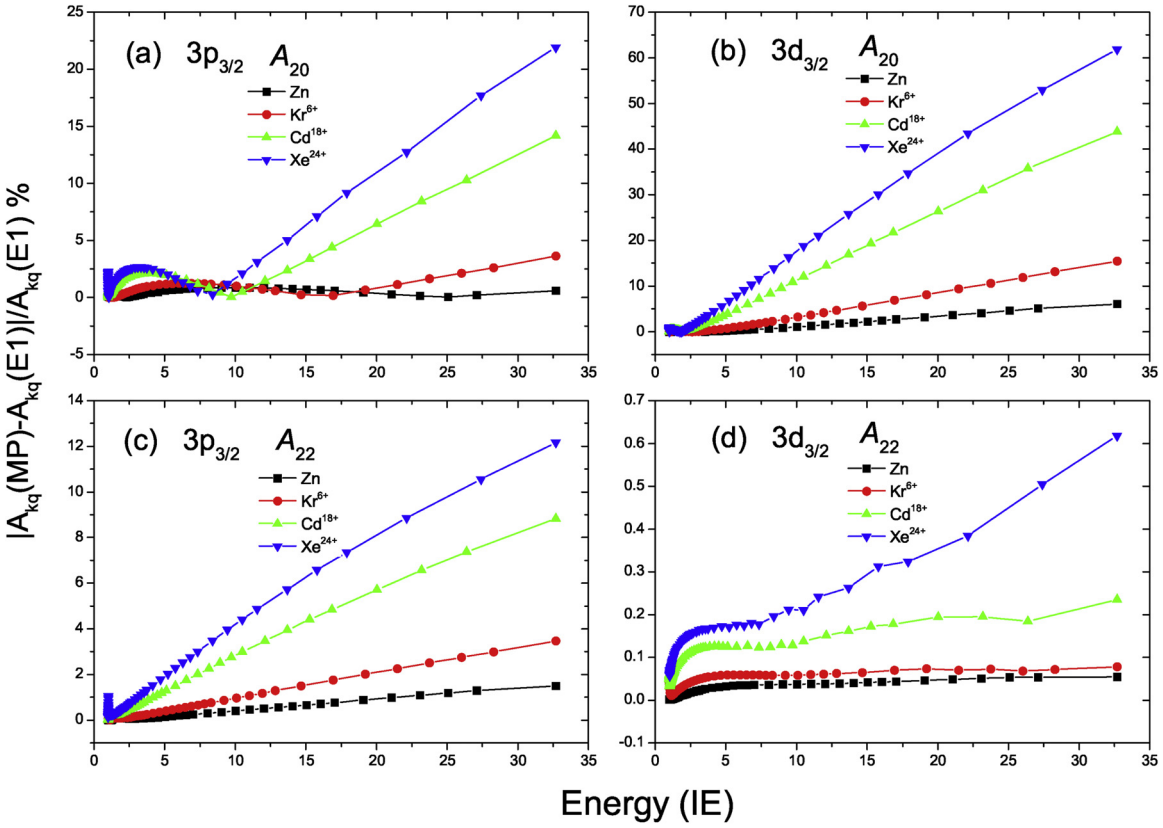

Fig. 4. Plot of the relative multipole contributions to the alignment parameters after PI of Zn and Zn-like ions by a linearly polarized photon against incoming photon energy.

alignment parameters grow with the increase of the incoming photon energy in a very similar way for all considered atomic shells. For the cross section, taking the inner-shell $3p_{3/2}$ vacancy as an example, at an incoming photon energy of 6IE, the MP result leads to an increase by a factor of 0.01 for compared to calculations in the $E1$ case, while at 32IE, the effects of multipole lead to a considerable increase for cross section, which could reach 15% of the $E1$ results. For the alignment parameter, the multipole effects increase the $A_{20}(A_{22})$ by almost 6.1% (0.054%), 15.5% (0.078%), 43.8% (0.23%), and 62.1% (0.62%) for the $3d_{3/2}$ vacancy of Zn and Zn-like Kr^{6+}, Cd^{18+}, and Xe^{24+} ions, respectively. We hope that with the development of experimental technology, such effects can be confirmed in experiments by measuring either the cross section or the alignment parameter after the process of PI of atom/ion by a linearly polarized photon.

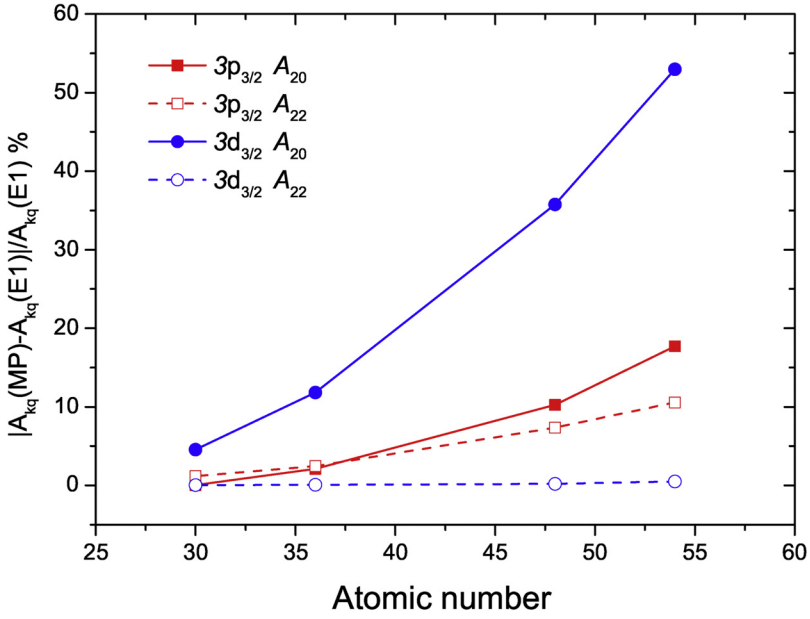

Fig. 5. Plot of the relative multipole contributions to the alignment parameters against atomic number. Here, the incoming photon energy is 25IE.

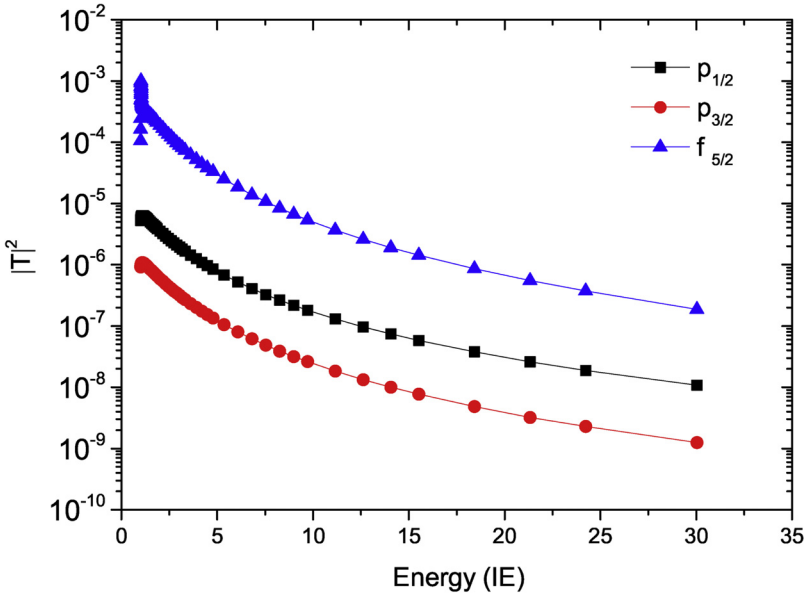

Fig. 6. The module of the reduced matrix element for the main PI channels as a function of incoming photon energy for Xe^{24+} ion.

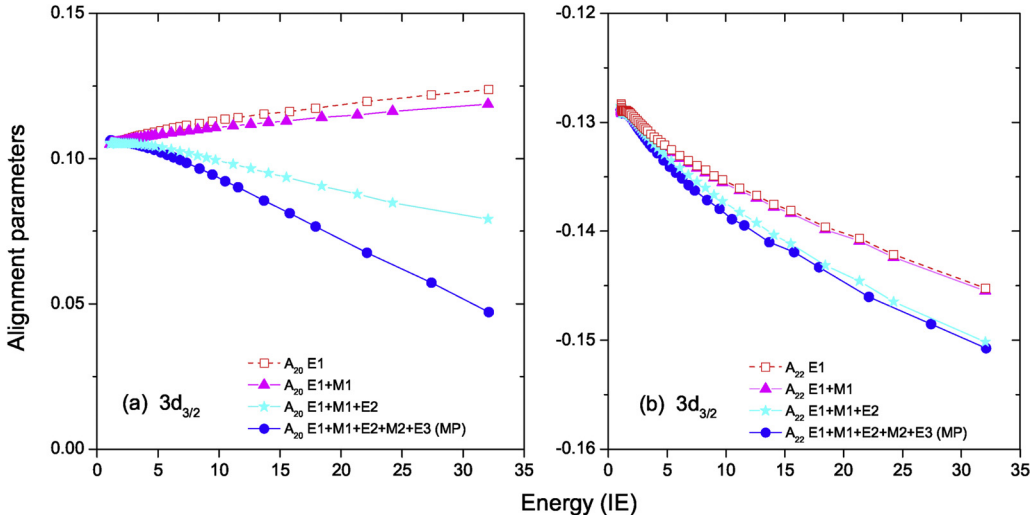

Fig. 7. Different multipoles contributions to the alignment parameters for the $3d_{3/2}$ vacancy of Xe^{24+} ion.

Author contribution

ZBC came up with the basic idea. KM carried out the calculations and plotted the graphs. Both authors drafted the manuscript (80% contribution). XLW, CCS, and KW contributed towards the polishing of the manuscript (20% contribution).

Acknowledgments

The authors acknowledge the support of the National Natural Science Foundation of China (Grant Nos. 11504421 and 11804112), the Natural Science Foundation of Anhui Province of China (1808085QA22), the Key Project for Young Talents in College of Anhui Province of China (Grant No. gxyqZD2016301), the Natural Science Foundation of the Higher Education Institutions of Anhui Province of China (Grant No. KJ2019A0610), and the Natural Science Foundation of the Higher Education Institutions of Anhui Province of China (Grant No. KJHS2015B01).

References

[1] S.D. Oh, J. McEnnen, R.H. Pratt, Phys. Rev. A 14 (1976) 1428.
[2] A. Bechler, R.H. Pratt, Phys. Rev. A 42 (1990) 6400.
[3] J.B. West, J. Phys. B 34 (2001) R45.
[4] J.B. West, Radiat. Phys. Chem. 70 (2004) 274.
[5] H. Kjeldsen, J. Phys. B 39 (2006) R325.
[6] I. Hofmann, Laser Part. Beams 8 (1990) 527.
[7] R.W.P. McWhirter, H.P. Summers, Applied Atomic Collision Physics vol. 2, Academic Press, New York, 1983, pp. 55–111.
[8] D.R. Flower, Atoms in Astrophysics, Plenum Press, New York, 1983, pp. 289–323.
[9] S. Flügge, W. Mehlhorn, V. Schmidt, Phys. Rev. Lett. 29 (1972) 7.
[10] D.C. Caldwell, R.N. Zare, Phys. Rev. A 16 (1977) 255.
[11] C. Pellegrini, A. Marinelli, S. Reiche, Rev. Mod. Phys. 88 (2016) 015006.
[12] K.S. Kahlon, H.S. Aulakh, N. Singh, R. Mittal, K.L. Allawadhi, B.S. Sood, J. Phys. B 23 (1990) 2733.
[13] H. Küst, U. Kleiman, W. Mehlhorn, J. Phys. B 36 (2003) 2073.
[14] W. Kronast, R. Huster, W. Mehlhorn, Z. Phys. D 2 (1986) 285–296.
[15] Y. Özdemir, R. Durak, M.R. Kacal, M. Kurudirek, Appl. Radiat. Isot. 69 (2011) 991–995.
[16] A. Hausmann, B. Kämmerling, H. Kossmann, V. Schmidt, Phys. Rev. Lett. 61 (1988) 2669.
[17] B. Kämmerling, A. Hausmann, J. Läuger, V. Schmidt, J. Phys. B 25 (1992) 4773.
[18] Z.M. Goodman, C.D. Caldwell, M.G. White, Phys. Rev. Lett. 54 (1985) 1156.
[19] W. Kronast, R. Huster, W. Mehlhorn, J. Phys. B 17 (1984) L51.
[20] G. Snell, E. Kukk, B. Langer, N. Berrah, Phys. Rev. A 61 (2000) 042709.

[21] S.J. Schaphorst, Q. Qian, B. Krässig, P. van Kampen, N. Scherer, V. Schmidt, J. Phys. B 30 (1997) 4003.
[22] U. Kleiman, B. Lohmann, J. Electron Spectrosc. Relat. Phenom. 131–132 (2003) 29–50.
[23] B. Lohmann, U. Kleiman, J. Phys. B 39 (2006) 271.
[24] E.G. Berezhko, N.M. Kabachnik, V.S. Rostovsky, J. Phys. B 11 (1978) 1749.
[25] N.F. Vorobyev, V.N. Kondratyev, N.M. Kabachnik, Nucl. Instrum. Methods B 27 (1987) 374–385.
[26] E.G. Berezhko, N.M. Kabachnik, J. Phys. B 10 (1977) 2467.
[27] A. Sharma, J. Electron Spectrosc. Relat. Phenom. 225 (2018) 1–4.
[28] R.A. Barrea, C.A. Perez, T.S. Plivelic, E.V. Bonzi, H.J. Sanchez, J. Phys. B 38 (2005) 839.
[29] Raj. Mittal, Vandana, Radiat. Phys. Chem. 51 (1998) 357.
[30] E.G. Berezhko, N.M. Kabachnik, V.V. Sizov, J. Phys. B 11 (1978) L421.
[31] A. Kumar, A.N. Agnihotri, D. Misra, S. Kasthurirangan, L. Sarkadi, L.C. Tribedi, J. Phys. B 48 (2015) 065202.
[32] M.K. Inal, A. Surzhykov, S. Fritzsche, Phys. Rev. A 72 (2005) 042720.
[33] A. Bechler, R.H. Pratt, Phys. Rev. A 42 (1990) 6400.
[34] J.W. Cooper, Phys. Rev. A 42 (1990) 6942.
[35] Ph.V. Demekhin, J. Phys. B 47 (2014) 025602.
[36] A. Bechler, R.H. Pratt, J. Phys. B 32 (1999) 2889.
[37] G.B. Pradhan, J. Jose, P.C. Deshmukh, L.A. LaJohn, R.H. Pratt, S.T. Manson, J. Phys. B 44 (2011) 201001.
[38] M.Ya. Amusia, N.A. Cherepkov, L.V. Chernysheva, Z. Felfli, A.Z. Msezane, J. Phys. B 38 (2005) 1133.
[39] L. Argenti, R. Moccia, J. Phys. B 43 (2010) 235006.
[40] W.R. Johnson, K.T. Cheng, Phys. Rev. A 63 (2001) 022504.
[41] V.V. Balashov, A.N. Grum-Grzhimailo, N.M. Kabachnik, Polarization and Correlation Phenomena in Atomic Collisions, Plenum Publisher, New York, 2000.
[42] P. Jönsson, X. He, C. Froese Fischer, I.P. Grant, Comput. Phys. Commun. 177 (2007) 597.
[43] Z.B. Chen, X.L. Guo, K. Wang, J. Quant. Spectrosc. Radiat. Transf. 206 (2018) 213.
[44] K. Wang, C.Y. Zhang, P. Jönsson, R. Si, X.H. Zhao, Z.B. Chen, X.L. Guo, C.Y. Chen, J. Yan, J. Quant. Spectrosc. Radiat. Transf. 208 (2018) 134.
[45] Z.B. Chen, K. Wang, X.L. Guo, J. Quant. Spectrosc. Radiat. Transf. 220 (2018) 28.
[46] K. Wang, P. Jönsson, J. Ekman, G. Gaigalas, M.R. Godefroid, R. Si, Z.B. Chen, S. Li, C.Y. Chen, J. Yan, Astrophys. J. Suppl. Ser. 229 (2017) 37.
[47] P. Jönsson, C. Froese Fischer, E. Träbert, J. Phys. B 31 (1998) 3497–3511.
[48] Z.B. Chen, K. Wang, J. Quant. Spectrosc. Radiat. Transf. 221 (2018) 31.
[49] Z.B. Chen, C.C. Sang, K. Wang, J. Quant. Spectrosc. Radiat. Transf. 225 (2019) 76–83.
[50] Z.B. Chen, C.Z. Dong, Eur. Phys. J. D 72 (2018) 101.
[51] T. Kämpfer, I. Uschmann, Z.W. Wu, A. Surzhykov, S. Fritzsche, E. Förster, G.G. Paulus, Phys. Rev. A 93 (2016) 033409.
[52] K. Ma, Z.B. Chen, L.Y. Xie, C.Z. Dong, Y.Z. Qu, J. Phys. B 50 (2017) 225202.
[53] L. Sharma, A. Surzhykov, M.K. Inal, S. Fritzsche, Phys. Rev. A 81 (2010) 023419.
[54] P. Jönsson, G. Gaigalas, J. Bieroń, C.F. Fischer, I.P. Grant, Comput. Phys. Commun. 184 (2013) 2197.
[55] Z.B. Chen, Phys. Plasmas 25 (2018) 052105.
[56] Z.B. Chen, H.W. Hu, K. Ma, X.B. Liu, X.L. Guo, S. Li, B.H. Zhu, L. Huang, K. Wang, Phys. Plasmas 25 (2018) 032108.
[57] K. Wang, S. Li, P. Jönsson, N. Fu, W. Dang, X.L. Guo, C.Y. Chen, J. Yan, Z.B. Chen, R. Si, J. Quant. Spectrosc. Radiat. Transf. 187 (2017) 375.
[58] Z.B. Chen, Phys. Plasmas 24 (2017) 122119.
[59] C. Froese Fischer, M. Godefroid, T. Brage, P. Jönsson, G. Gaigalas, J. Phys. B 49 (2016) 182004.
[60] Z.B. Chen, Eur. Phys. J. D 72 (2018) 67.
[61] Z.B. Chen, K. Ma, H.W. Hu, K. Wang, Phys. Plasmas 25 (2018) 072120.
[62] S. Verdebout, C. Nazé, P. Jönsson, P. Rynkun, M. Godefroid, G. Gaigalas, At. Data Nucl. Data Tables 100 (2014) 1111–1155.
[63] S. Fritzsche, Comput. Phys. Commun. 183 (2012) 1525.
[64] G. Snell, E. Kukk, B. Langer, N. Berrah, Phys. Rev. A 61 (2000) 042709.
[65] S.B. Whitfield, C.D. Caldwell, D.X. Huang, M.O. Krause, J. Phys. B 25 (1992) 4755.
[66] B. Kämmerling, B. Krässig, V. Schmidt, J. Phys. B 23 (1990) 4487.
[67] B. Kämmerling, V. Schmidt, Phys. Rev. Lett. 67 (1991) 1848.
[68] B. Kämmerling, V. Schmidt, J. Phys. B 26 (1993) 1141.
[69] S.J. Schaphorst, Q. Qian, B. Krässig, P. van Kampen, N. Scherer, V. Schmidt, J. Phys. B 30 (1997) 4003.